



1 **Measured methane emissions from a metropolitan wastewater**
2 **treatment lagoon in Victoria Australia are substantially**
3 **higher than report emissions based on emission factors**

4 Mei Bai^{1,*}, Pieter de Jong², Ellen Tao², Deli Chen¹

5 ¹School of Agriculture, Food and Ecosystem Sciences, Faculty of Science, The University of Melbourne,
6 Parkville, Victoria, 3010, Australia

7 ²Melbourne Water Corporation, Docklands, Victoria 3008, Australia

8 *Corresponding to:* Mei Bai, mei.bai@unimelb.edu.au

9

10 **Abstract.** Wastewater treatment facilities contribute ~8 % of global anthropogenic methane (CH₄)
11 emissions. Accurate measurements of CH₄ emissions not only improve greenhouse gas (GHG) emission
12 estimates from the facilities but also expand our understanding of operational impact on emissions, thus
13 enabling the development of effective mitigation strategies. In this study, CH₄ emissions were measured
14 during summer and winter seasons at an aerobic lagoon at a large sewage treatment plant in Australia.
15 Line-averaged CH₄ concentrations were measured by open-path lasers and CH₄ fluxes were calculated
16 using inverse-dispersion modelling. Methane fluxes showed temporal and spatial variations over the
17 measurement periods, and correlated with wastewater dissolved methane, flow rate, and aerator
18 operation. The annual GHG emission of 79,593 tCO₂-e yr⁻¹, represents ~25 % of CH₄ production
19 captured by the anaerobic digestion pot, and is approximately 2–3 times higher than the National
20 Greenhouse and Energy Reporting Scheme (NGERS) reported emissions of the aerobic lagoon.

21

22 **Keywords:** methane emissions, sewage treatment lagoon, surface aerators, inverse-dispersion
23 modelling, open-path laser sensors

24

25 **Abbreviations:** BOD, biological oxygen demand, COD, chemical oxygen demand, IDM, inverse-
26 dispersion modelling, NGERS, National Greenhouse and Energy Reporting Scheme, OPL, open-path
27 laser, WWTPs, wastewater treatment plants

28

29 **1. Introduction**

30 Wastewater treatment plants (WWTPs) are a significant source of greenhouse gas (GHG) emissions resulting
31 from the environments that have high supply of organic matter and nutrients (Czepiel et al., 1993; Daelman et al.,
32 2012). Substantial methane (CH₄) emissions from wastewater treatment facilities have been reported (Guisasola
33 et al., 2008; Song et al., 2023), with this sector contributing to ~5–8 % of global anthropogenic CH₄ emissions
34 (Ye et al., 2022), following livestock (32 %), oil and gas (25 %), land fill (13 %), and coal mine (11 %). Methane
35 contributes to climate change with a global warming potential 27 times that of carbon dioxide (CO₂) in a 100–
36 year time span and 80 times CO₂ considering a 20–year timeframe (Ipcc, 2021). To achieve the goal of the Paris
37 Agreement (e.g., limiting global temperature rise to well below 2 °C above pre-industrial levels), reducing



38 WWTP's GHG emissions is an important climate action to help to prevent the worst impacts of climate change.
39 Furthermore, assessing the environmental impacts of GHGs, has become a necessity for the long-term
40 sustainability of WWTPs (Mohsenpour et al., 2021). To reduce GHG emissions from WWTPs and achieve the
41 Australia Water sector's goal of net zero emissions by 2035, it requires a better understanding of current GHG
42 emission rates from facilities, as well as an evaluation of the main drivers of emissions, to implement appropriate
43 mitigation measures. Currently there are large uncertainties in estimating these emissions, as WWTPs use
44 generalised, default emission factors (National Greenhouse and Energy Reporting Scheme (NGERS), method 2)
45 (Bartram et al., 2019; Nger, 2022), which may not accurately represent local conditions and the specific
46 management practices.

47 Across various nations, anaerobic ponds are commonly used as the first step in municipal sewage treatment. Raw
48 sewage enters anaerobic ponds and settles into different layers, with a liquid layer over the sludge to prevent
49 oxygen from reaching it during microbial digestion. Anaerobic microbes present in the sludge digest the organic
50 matter in influent raw sewage and settle to the bottom of the pond along with organic and inorganic solids. Sludge
51 can be removed and reused for land application. Aerobic ponds are used following the anaerobic ponds where
52 aerators are deployed to introduce air into the water column. This allows for aerobic respiration to occur, where
53 oxygen and other microbes in the wastewater are mechanically churned, helping to break down organic matter.
54 The bacterial-containing chunks settle to the bottom of the pond. During these processes, CH₄, N₂O, and NH₃
55 emissions are emitted into the atmosphere.

56 This study focussed on measuring CH₄ emissions at a large lagoon-based sewage treatment facility in Victoria,
57 Australia. It occupies a site of more than 10,000 ha, serving up to 2.5–3 million residents. The area of focus for
58 this emissions measurement research is known as 25W Pond 1, which is adjacent to a covered anaerobic digestion
59 pot, where the raw sewage influent undergoes preliminary treatment. The majority of the treated wastewater after
60 the anaerobic pot enters directly into the Pond 1 (25W) for aerobic treatment with surface aerators, the rest of the
61 wastewater is pumped into an anoxic-aerobic activated sludge plant for secondary treatment. The waste activated
62 sludge generated from the activated sludge plant is returned to the Pond 1 for treatment. The 25W Pond 1 system
63 has 53 surface aerators distributed across the pond (the layout of aerators is shown in Supplementary Materials),
64 and the aerators operational time is often controlled by the flow rate. Furthermore, the aerators (when on) increase
65 the oxygen content in their immediate vicinity, while the water region far from the aerators has less or no oxygen
66 (Nguyen et al., 2024). This operating regime contributes to the spatial and temporal variation of the conditions
67 within the pond (Li et al., 2024; Liu et al., 2023). This makes it very challenging to accurately measure GHG
68 emissions (Delre et al., 2017).

69 Different measurement technologies have been reported for measuring GHG emissions in the WWTPs either for
70 integration emission quantification or identification of specific facilities (He et al., 2025). In many jurisdictions
71 the chamber technique is a regulatory standard for direct gas emission measurements (Ye et al., 2022; Morales-
72 Rico et al., 2024; Parravicini et al., 2022). However, chamber measurements are susceptible to the disturbances
73 that result from isolating the source inside a chamber (e.g. it is challenging to measure the emissions from surface
74 aerators (Morales-Rico et al., 2024)). The small measurement footprint of chambers (covering less than 1 m² of
75 surface) is likely to be a tiny fraction of the source area. Chambers are also poorly suited for long-term
76 measurements due to the labour cost.



77 World-wide efforts are underway to implement measurement methodologies that are more accurate than chambers
78 (and cheaper and logistically simpler to use) (Reinelt et al., 2017; Yver Kwok et al., 2015; Jensen et al., 2017;
79 Delre et al., 2017; Samuelsson et al., 2018). One such alternative is the inverse-dispersion modelling (IDM)
80 approach (Flesch et al., 2011), which is the basis of this study. This technique follows the simple idea that an
81 emission source increases the downwind gas concentration, and that a measurement of downwind concentration
82 (above the upwind background level) can be used to quantify the emission rate from the source area. The
83 correlation between the emission rate and concentration is calculated with an atmospheric dispersion model
84 (Flesch et al., 1995). IDM is a non-interference/non-intrusive technique that does not alter the measurement
85 environment. It has modest measurement requirements and is well suited for long-term deployment. We recently
86 reported our studies of measuring CH₄, N₂O, and NH₃ emissions from a sludge drying pan at a WWTP using IDM
87 methods coupled with open-path spectroscopic techniques (Bai et al., 2023; Bai et al., 2025).
88 The objectives of this study are to measure CH₄ emissions from the 25W Pond 1 using IDM coupled with open-
89 path laser techniques, explore the main drivers of emissions from the facility, and validate the NGERs estimate.
90

91 **2. Materials and Methods**

92 **2.1 Experimental site**

93 This study was conducted at the sewage treatment plant, located in Victoria, Australia. One of two identical
94 aerobic treatment lagoons, 25W Pond 1 was chosen for this study. Wastewater after being treated at from the
95 anaerobic Pot flows directly into 25W Pond 1, and flows through the pond in an east-west direction. The 25W
96 Pond 1 has dimension of 250 × 1010 × 3 m (width × length × depth) (Fig. 1). There are also several lagoons
97 located on the south of the Pond 1, while to the north of Pond 1 the terrain is flat, covered with short grass, and
98 there are no trees or buildings nearby. Further north, there is a corn field, about a few hundred meters north of the
99 pond. A sludge drying pan area is located ~200 m to the west of the pond. This layout allows for CH₄
100 measurements when there are winds tending from the north, because to the north within a radius of a couple of
101 hundred meters, there are no other CH₄ sources interfering with the measurements. The average
102 minimum/maximum ambient temperature was approximately 18 °C and 26 °C for summer, 12 °C and 19 °C for
103 winter, respectively. A total of 1.4 and 37.4 mm of precipitation was observed over the summer and winter
104 measurement period, respectively.

105

106 Figure 1

107

108 **2.2 CH₄ concentrations measured with open-path laser sensors**

109 Three open-path lasers (OPL) were deployed in each campaign measuring line-average CH₄ concentration (in
110 ppm-m). Two of the three laser sensors used in this study were from Unisearch Associates Inc. Canada
111 (LasIRView, OPL_C33, OPL_C34), the third laser was from Boreal Laser Inc. Canada (Gasfinder 2.0,
112 OPL_C1013). The concentration sensor sends a collimated beam from a tunable infrared laser diode to the retro
113 reflector mirror, from which the beam is reflected back to the receiver optics and a detector. The outgoing beam
114 is altered by CH₄ molecules over the measurement path (between the laser and retro reflector), giving a measure



115 of concentration. Line-averaged CH₄ concentration is obtained every few seconds. The precision of CH₄
116 concentration at a 100 m path length is: < 1 ppb for the Unisearch laser, 20 ppb for the Boreal laser.
117 To avoid surrounding ponds contributing to the emission of target source Pond 1, our experimental layout was
118 designed for only northerly winds, and data collected with other wind directions was not counted for the flux
119 calculation. In each campaign, two lasers were set up at the south of the pond to measure the downwind
120 concentrations: OPL_C33 was located the western side of the pond (west laser) and OPL_C1013 was located the
121 eastern side (east laser), close to the anaerobic Pot cover area. The third laser OPL_C34 (background laser) was
122 located at the north of the pond measuring the upwind concentration (Fig. 1).
123 Each laser and retro reflector were mounted on a separate tripod at approximate 1.50 m above the ground, with
124 the pathlength of 100–150 m between the laser and retro reflector. Each OPL was powered by a 12-v battery
125 coupled with solar panels. Prior to the measurements, three lasers were conducted cross-calibration on site for at
126 least 48 hours to examine their stability and performance under same climate conditions. Gas emission
127 measurements were begun from 8 February to 12 March 2024 for the summer campaign, and from 15 August to
128 5 October 2024 for the winter campaign. Measurements from both campaigns are included in this paper.

129

130 **2.3 Pond 1 wastewater samples collected using drone**

131 To examine the Pond 1 effluent chemical and physical property and understand how these factors are associated
132 with the flux measurements, wastewater samples were collected in September using a drone along the middle of
133 the pond at 5, 50, 100, 150, 200, 275, 350 and 500 m from the Pot covered area (sampling locations are shown in
134 Supplements Fig. 1). For each sample, the temperature, redox, pH, and dissolved oxygen were analysed
135 immediately on site. Subsamples (850 mL each) were also taken at each location and analysed in the laboratory
136 for other properties analysis.

137

138 **2.4 CH₄ flux calculations using IDM technique**

139 The IDM technique is a classic micrometeorological method that calculates emissions from gas measurements
140 taken in the free air. The micrometeorological methods are generally preferable to other approaches, as they are
141 non-intrusive techniques that are suitable for long-term measurements. Consider a treatment pond that is emitting
142 gas to the atmosphere at an unknown rate Q , which causes the average gas concentration (C) downwind of the
143 pond to rise above the background value (C_b). In the IDM technique, the measurement ($C - C_b$) is used to determine
144 Q with the aid of an atmospheric dispersion model (Windtrax). Because the Q vs ($C - C_b$) relationship depends on
145 wind conditions, one must also make wind measurements.

146 In this study, open-path CH₄ sensors were located to the south and north of the experimental pond. During
147 northerly winds, this configuration allowed upwind (*Cupwind*) and downwind (*Cdownwind*) measurements from
148 the experimental pond, but not the southern ponds. Following Flesch et al. (2004), the CH₄ flux Q_{IDM} is calculated
149 using IDM method following the equation (Eq.1):

$$150 \quad Q_{IDM} = (C_{downwind} - C_{upwind}) / (C/Q)_{sim} \quad (1)$$

151 where Q_{IDM} is the CH₄ gas emission rate ($\mu\text{g m}^{-2} \text{s}^{-1}$), and $C_{downwind}$, C_{upwind} is the line-average gas
152 concentrations (in ppm) measured by downwind and upwind laser sensor, respectively (Fig. 1). The value of



153 $(C/Q)_{\text{sim}}$ is the simulated ratio of line-average concentration and emission rate, calculated by WindTrax modelling
154 based on the ambient temperature and pressure, wind statistics, and atmospheric turbulent parameters.

155

156 A three-dimensional (3-D) sonic anemometer (CSAT-3, Campbell Scientific, Logan, Utah, USA) coupled with
157 a datalogger (CR23X, Campbell Scientific, Logan, Utah, USA) was located at the south of the Pond 1 at a height
158 of 2.34 m above the ground (Fig. 1), to record wind statistics at a frequency of 10-Hz that are needed for IDM
159 calculation. Fifteen-min statistics includes the friction velocity (u^* , m s^{-1}), turbulent velocity (u , v , w , T), and its
160 variance (u^2 , v^2 , w^2 , T^2) and covariance (uT , uv , uw , vT , vw , wT) in three dimensions, as well as ambient
161 temperature ($^{\circ}\text{C}$), wind speed (m s^{-1}), and wind direction. Ambient pressure (mb) and rainfall (mm) were obtained
162 from Bureau of Meteorology.

163

164 The concentrations of CH_4 were averaged into 15-min intervals then merged with wind variables as inputs for the
165 IDM flux calculation using SAS software (SAS 9.4, SAS Institute Inc. Cary, NC, USA). The atmospheric
166 turbulent parameters including Obukhov stability length (L , m), surface roughness (z_0 , m), and turbulent velocity
167 fluctuation ($\sigma u/u^*$, $\sigma v/u^*$, and $\sigma w/u^*$) were also calculated for the IDM simulation.

168

169 **2.5 CH_4 flux calculation filtering criteria**

170 Following Flesch et al. (2016), the data for CH_4 emission calculations using the IDM methods were not counted
171 when:

- 172 1) atmospheric turbulent conditions were poor: $u^* < 0.1 \text{ m s}^{-1}$, $|L| < 2 \text{ m}$, $z_0 > 0.05 \text{ m}$,
- 173 2) the laser light level returned by the retro reflector was $< 6,000$ or $> 12,000$,
- 174 3) the relationship between the measured external and reference signal R^2 was < 96 ,
- 175 4) The difference in concentration between the upwind measurement and background level simulated by IDM
176 (WindTrax model) was $> 0.02 \text{ ppm}$,
- 177 5) The upwind laser concentration measurement was $< 1.8 \text{ ppm}$,
- 178 6) The percentage of source area covered by the touchdowns was $< 20 \%$,
- 179 7) Wind direction was $> 40^{\circ}$ and $< 330^{\circ}$

180

181 **2.6 Average Pond 1 CH_4 flux calculation**

182 The classic way to do post-stratification when using stratified sampling is to weight the estimate by the area that
183 each strata represents (i.e., take a weighted average). In summer campaign, the pond was divided into two strata
184 of similar size, the total emission was thus $(0.5 \text{ times flux}_1 + 0.5 \text{ times flux}_2) \times \text{total pond area}$. Because the east
185 laser was much closer to the Pot end covered area for the winter campaign, we used a weight of 0.67 for the west
186 laser (flux 1) and a lower weight of 0.33 for the east laser (flux 2), therefore, the total emission was thus $(0.67$
187 $\text{ times flux}_1 + 0.33 \text{ times flux}_2) \times \text{total pond area}$. For a more conservative estimate, a weight of 0.25 was used
188 for east laser and 0.75 for west laser, the total emission was thus $(0.75 \text{ times flux}_1 + 0.25 \text{ times flux}_2)$.

189 **2.7 CH_4 flux uncertainty**

190 There are four sources of uncertainty in our flux estimate: instrument precision ($\pm 0.02 \%$), inversion dispersion
191 model ($\pm 20 \%$) (Laubach and Kelliher, 2005), sampling uncertainty (i.e., the s.e. calculated using the number of



192 observations and standard deviation among the 15-min measurements, which contributes around 1.2 to 4.0 %),
193 and the pond area represented by each laser in our weighted average (50–50 % for the summer campaign; from
194 25 to 33 % for laser 1013 and 75 to 67 % for laser 33 for the winter campaign, which corresponds to a 5 % relative
195 error for winter and 0 % error for summer). These four sources of uncertainty are added in quadrature ($\sqrt{e_1^2$
196 $+ e_2^2 + e_3^2 + e_4^2}$), where the e_i 's are the different error terms) to propagate the uncertainty and get our final
197 estimates: $417.0 \mu\text{g m}^{-2}\text{s}^{-1}$ (± 20.4 %, total uncertainty) in summer and $349.1 \mu\text{g m}^{-2}\text{s}^{-1}$ (± 20.7 %, total uncertainty)
198 in winter. The average emission for Pond 1 over the two campaigns is $383.1 \mu\text{g m}^{-2}\text{s}^{-1}$ (± 20.5 %, total uncertainty).
199 Note that the total uncertainty is dominated by the inverse-dispersion model term as the terms are added in
200 quadrature.

201

202 3. Results and Discussion

203 3.1 Spatial and temporal variations of CH₄ fluxes

204 Fifteen-minute CH₄ fluxes from Pond 1 varied spatially between the eastern and western pond areas (Fig. 2).
205 Higher fluxes were observed at eastern pond area, ranged from ~200 to over $1900 \mu\text{g m}^{-2}\text{s}^{-1}$, and lower fluxes
206 ranged from ~13 to over $570 \mu\text{g m}^{-2}\text{s}^{-1}$ were observed at western pond area. Furthermore, a clear 24-h diurnal
207 pattern in the fluxes was observed at the eastern pond area, with lower emissions around midday and higher
208 emissions at night-time or early morning. This diurnal pattern of maximum CH₄ emission at 8 am was also
209 reported in Glaz et al. (2016). In contrast, no obvious diurnal pattern of the emissions was observed at the western
210 measurement location.

211 Daily averaged CH₄ fluxes varied among the seasons (Fig. 2). In the summer season, the daily average of CH₄
212 flux was $252.0 (\pm 9.4, n = 139)$ (\pm s.e. for sampling uncertainty, n, observation numbers) and $582.1 (\pm 23.3, n =$
213 $185) \mu\text{g m}^{-2}\text{s}^{-1}$ from the western and eastern pond area over the 5-week measurement period, respectively. In the
214 winter season, the daily averaged CH₄ flux was $134.7 (\pm 2.3, n = 797)$ and $874.2 (\pm 10.6, n = 692) \mu\text{g m}^{-2}\text{s}^{-1}$ from
215 western and eastern pond area over the 7-week measurement period, respectively. The emissions at eastern pond
216 area were ~2–6 times higher than that at western pond area, during both winter and summer measurements. The
217 much higher eastern flux measurement in the winter campaign was mainly due to the laser measurement location
218 being much closer to the anaerobic Pot covered area than during the summer measurement campaign. In contrast,
219 the laser's locations at the western pond area remained the same during both summer and winter campaigns and
220 the pond measurements were higher in summer than that in winter by 46 %.

221 The measured winter flux at western pond area was much higher than the higher range of the reports, e.g., the
222 anerobic ponds in Australia ($7 \pm 1 \text{ g m}^{-2} \text{ day}^{-1}$) (Hernandez-Paniagua et al., 2014), duckweed treatment ponds of
223 $1276 \pm 299 \text{ mg CH}_4 \text{ m}^{-2} \text{ d}^{-1}$ in the US (Sims et al., 2013), organic matter enriched sludge treatment wetlands of
224 $1900 \text{ mg CH}_4 \text{ m}^{-2} \text{ d}^{-1}$ in Norway (Søvik and Kløve, 2007), and $5400 \text{ mg CH}_4 \text{ m}^{-2} \text{ d}^{-1}$ Spain (Uggetti et al., 2012).
225 Different measurement techniques, wastewater composition, climate conditions and operation management could
226 introduce variability of methane fluxes (Reinelt et al., 2017).

227

228 Figure. 2

229



230 **3.2 Main drivers of CH₄ fluxes from 25W Pond 1**

231 **3.2.1 Wastewater chemical and physical properties and flow rate**

232 The composition and load of the wastewater played important roles in the spatiotemporal dynamics of gas
233 emissions (Glaz et al., 2016). The wastewater sampling collected along the middle section of Pond 1 in September
234 showed that dissolved methane, biological oxygen demand (BOD), chemical oxygen demand (COD), and
235 wastewater temperature decreased with distance from the Pot covered area (Fig. 3), in contrast, dissolved oxygen,
236 pH, and redox positively correlated with distance from the anaerobic Pot covered area ($P < 0.05$). This decreasing
237 trend of dissolved methane would explain the spatial variation of pond emissions and the difference in measured
238 CH₄ fluxes between the eastern and the western part of the pond. Linear correlations with correlation coefficient
239 (R) and P value are shown in Figure 4.

240 Wastewater flow rates (Fig. 5) showed a 24-h diurnal trend through the pot-pond area: lower flow rates before
241 midday and higher flow rates in the evening and early morning. The winter measurement as an example is shown
242 in Figure 5. This diurnal pattern of flow rates was similar to the CH₄ flux diurnal variation, but the latter showed
243 a time lag of ~1–2 h (Fig. 5, red dots and red line). This is not surprising as, together, Pond 1 and the Pot covered
244 area are a large area, and it takes 1–2 h for the wastewater to flow into the area where the laser measures the
245 footprints of emissions. Besides this, hourly mean fluxes from the eastern pond area were positively correlated to
246 hourly mean wastewater flow rates ($R = 0.49$, $P < 0.001$). This relationship was also reported in Glaz et al. (2016).
247 However, the mean flux from the western pond area did not show an obvious correlation to the flow rate. As stated
248 previously, the emission variation was associated with wastewater dissolved methane concentrations. At the
249 western end of the pond the concentration of dissolved methane was negligible and therefore, there were lower
250 CH₄ fluxes.

251

252 Figure 3

253 Figure 4

254 Figure 5

255

256 **3.2.2 Aerators operation**

257 The surface aerators closest to two downwind measurement lasers were examined, and the fluxes were compared
258 before the surface aerators were all switched off, when they were off, and when they were switched on again. For
259 the aerators close to the east laser, the hourly fluxes were 830.2, 296.8, 1453.0 $\mu\text{g m}^{-2} \text{s}^{-1}$ for before these aerators
260 were all switched off, when they were off and when they were switched on again, respectively, on 23 August, and
261 1139.8, 251.2, 766.0 $\mu\text{g m}^{-2} \text{s}^{-1}$, respectively, on 6 September 2024. In contrast, on the west end of the pond, the
262 hourly fluxes were 90.0, 81.0 and 130.0 $\mu\text{g m}^{-2} \text{s}^{-1}$ on 23 August for the before, during and after the off event,
263 respectively, and 191.0, 121.0 and 125.0 $\mu\text{g m}^{-2} \text{s}^{-1}$ on 6 September 2024, respectively. Therefore, the surface
264 aerators off events at the eastern pond area substantially decreased the emissions flux by 80 %.

265

266 **3.2.3 25W Pond 1 daily CH₄ flux and annual GHG emissions**

267 The average daily CH₄ flux from 25W Pond 1 was 8.79 and 7.36 t day^{-1} over the summer and winter measurement
268 period, respectively, by taking the mean of both fluxes at eastern and western pond area and multiplying by the
269 total pond area (~244,000 m^2) (Table 1). It was found that during the summer campaign, the fluxes over the



270 western pond area were almost 2 times higher than that of the winter campaign (252 vs $134 \mu\text{g m}^{-2} \text{s}^{-1}$). This is
271 likely associated with the sludge dredging events at Pond 1 between June and July 2024 (only weeks before the
272 start of winter campaign). The dredging took place at the location where the western laser was measuring. It
273 should also be noted that prior to the dredging in 2024, Pond 1 was last dredged in April–August 2023, which was
274 approximately 6 months before the summer campaign. This means that removed sludge could have resulted in the
275 lower emissions at 25W Pond 1 during the winter campaign. Noting that most emissions measured at the western
276 pond area are likely from the sludge rather than the wastewater given the very low dissolved methane
277 concentration in the western pond area.

278 Methane emissions from Pond 1 showed temporal and spatial variations over the measurement periods, with an
279 average of $381.1 \mu\text{g m}^{-2} \text{s}^{-1}$, equivalent to annual CH_4 emission of $2,948 \text{ t}$ (Table 1). The annual CH_4 emission was
280 then calculated as CO_2 equivalent ($\text{CO}_2\text{-e}$) by multiplying this value by a factor of 27 (CH_4 's global warming
281 potential in 100 years) (Ipcc, 2021), resulting in an annual GHG emission of $79,593 \text{ tCO}_2\text{-e yr}^{-1}$ (Table 1). The
282 emissions at the eastern pond area were comparable to the measurements from wastewater treatment facilities in
283 the US using remote sensing techniques (Thorpe et al., 2021).

284 According to the daily average effluent flow of $108.6 \text{ ML day}^{-1}$, we calculated net daily COD change in Pond 1
285 (ΔCOD , mg L^{-1}) using the difference in the COD value between the average influent COD value (measured at the
286 east end) and the average effluent COD value at the outlet. The ΔCOD for the summer and winter campaign was
287 306.2 and $379.8 \text{ ML day}^{-1}$, corresponding to 36.58 and $41.25 \text{ tCOD day}^{-1}$ processed by the Pond 1, respectively.
288 Therefore, the accumulative CH_4 flux per tCOD change accounted for $178.4 \text{ kgCH}_4 \text{ t}^{-1} \Delta\text{COD}$ for winter campaign,
289 comparable to the value of $240.3 \text{ kgCH}_4 \text{ t}^{-1} \Delta\text{COD}$ for summer campaign (Table 1).

290

291 Table 1

292

293 The average annual flux as a proportion of production ranged from 23.4 to 25.3 %, reflecting that the measured
294 emissions are approximately 25 % of the CH_4 captured by the anaerobic Pot. Our measurements are $\sim 3.2\text{--}3.4$
295 times higher than the NGERs reported emissions from Pond 1 (adopting the emissions factor of Unmanaged
296 Aerobic Lagoon, Method 2, NGERs) which averaged $36,843 \text{ tCO}_2\text{-e yr}^{-1}$ for financial years 2023 and 2024 (Table
297 2). These results are comparable to other studies on CH_4 emissions from WWTPs, which found that measured
298 emissions were almost 2 times IPCC (Intergovernmental Panel on Climate Change)/EPA estimates that use
299 emission factors (Moore et al., 2023; Song et al., 2023).

300

301 Table 2

302

303 In Australia, approximately 737 of the 1,234 WWTPs primarily use treatment ponds, accounting for ~ 60 % of
304 the total WWTPs nationwide. The NGERs estimate across the 737 WWTPs is $18.5 \text{ MtCO}_2\text{-e yr}^{-1}$, based on our
305 study the actual national GHG emissions from the treatment lagoons could be considerably higher than the
306 estimate. In fact, while fugitive CH_4 emissions from coal, oil, and gas plants have been the focus in Australia and
307 globally, little attention has been paid to CH_4 emissions from sewage treatment ponds. The potentially
308 underestimated CH_4 emissions are often overlooked in climate change calculations. Meanwhile, climate change-
309 induced warming in Australia and Melbourne's growing population will likely enhance CH_4 emissions from



310 WWTPs. These issues must be addressed, and concrete actions to reduce GHG emissions from the wastewater
311 sector are urgently needed.

312

313 **4. Conclusions and recommendations**

314 Methane emissions from 25W Pond 1 showed the temporal and spatial variations over the measurement periods.
315 The average annual flux as a proportion of CH₄ production ranged from 23.4 % to 25.3 %, reflecting that the
316 measured emissions are approximately 25 % of the methane captured by the Pot. Our measurements are ~3 times
317 higher than the NGERs estimate. We therefore recommended that the options for mitigating CH₄ emissions
318 include examining the impacts of changing management practices. Such practices could involve increasing the
319 dredging frequency of Pond 1, increasing the efficacy of capturing CH₄ from the covered area (e.g., by extending
320 its length), optimizing the aerator operating time to prolong the period that dissolved methane remains in the
321 wastewater, or adding substances to the pond (e.g. microalgae). However, in practice these proposals might not
322 be viable options. In the long run, to substantially reduce fugitive CH₄ emissions from WWTPs that contributes
323 to achieving carbon neutrality, it will be necessary to implement a new primary treatment plant and move away
324 from the current anaerobic treatment followed by aerobic pond design.

325 To facilitate the investigation on methane reduction, a study of the microbial community within the wastewater
326 and sludge will help to better understand the methane production processes. In addition, this study has shown that
327 inverse-dispersion modelling combined with open-path spectroscopic techniques are useful tools to continually
328 monitor emissions at a large scale. Measuring a suite of gas emissions including CH₄, N₂O, and NH₃, would better
329 allow the development of effective mitigation strategies. This is especially important once the methane oxidizers
330 and producers in a wastewater treatment pond are identified.

331

332 **5. Author contributions**

333 MB, PJ, DC designed the experiments and MB carried them out. MB prepared the manuscript with
334 contributions from all co-authors.

335

336 **6. Acknowledgements**

337 This study is funded by Melbourne Water. We sincerely acknowledge the students and staff from the University
338 of Melbourne for their support and assistance during this study.

339

340 **7. Data Availability**

341 The data will be available before publication.

342

343 **8. Competing interests**

344 The authors declare that they have no conflict of interest.

345



346 **9. References**

- 347 Bai, M., Wang, Z., Lloyd, J., Seneviratne, D., Flesch, T., Yuan, Z., and Chen, D.: Long-term onsite
348 monitoring of a sewage sludge drying pan finds methane emissions consistent with IPCC
349 default emission factor, *Water Res. X*, 19, 100184, <https://doi.org/10.1016/j.wroa.2023.100184>,
350 2023.
- 351 Bai, M., Wang, Z., Seneviratne, D., Lloyd, J., De Jong, P., Ye, L., and Chen, D.: Substantial
352 ammonia emissions from sludge drying pans in wastewater treatment plants, *Nat. Water*, 3,
353 1125-1132, 10.1038/s44221-025-00479-8, 2025.
- 354 Bartram, D., Short, M. D., Ebie, Y., Farkaš, J., Gueguen, C., Peters, G. M., Zanzottera, N. M., and
355 Karthik, M.: Wastewater Treatment and Discharge. In '2019 Refinement to the 2006 IPCC
356 Guidelines for National Greenhouse Gas Inventories. Vol. 5. Waste'. Ch. 6. Prepared by the
357 National Greenhouse Gas Inventories Programme, International Panel on Climate Change,
358 2019.
- 359 Czepiel, P. M., Crill, P. M., and Harriss, R. C.: Methane emissions from municipal wastewater
360 treatment processes, *Environ. Sci. Technol.*, 27, 2472-2477, 10.1021/es00048a025, 1993.
- 361 Daelman, M. R. J., van Voorthuizen, E. M., van Dongen, U. G. J. M., Volcke, E. I. P., and van
362 Loosdrecht, M. C. M.: Methane emission during municipal wastewater treatment, *Water Res.*,
363 46, 3657-3670, <https://doi.org/10.1016/j.watres.2012.04.024>, 2012.
- 364 Delre, A., Mønster, J., and Scheutz, C.: Greenhouse gas emission quantification from
365 wastewater treatment plants, using a tracer gas dispersion method, *Sci. Total Environ.*, 605,
366 258, 2017.
- 367 Flesch, K. T., Baron, V., Wilson, J., Griffith, D. W. T., Basarab, J., and Carlson, P.: Agricultural gas
368 emissions during the spring thaw: Applying a new measurement technique, *Agric. Forest
369 Meteorol.*, 221, 111-121, 10.1016/j.agrformet.2016.02.010, 2016.
- 370 Flesch, T. K., Desjardins, R. L., and Worth, D.: Fugitive methane emissions from an agricultural
371 biodigester, *Biomass and Bioenergy*, 35, 3927-3935,
372 <https://doi.org/10.1016/j.biombioe.2011.06.009>, 2011.
- 373 Flesch, T. K., Wilson, J. D., and Yee, E.: Backward-time Lagrangian stochastic dispersion
374 models and their application to estimate gaseous emissions, *J. Appl. Meteorol.*, 34, 1320-1332,
375 10.1175/1520-0450(1995)034<1320:BTLSDM>2.0.CO;2, 1995.
- 376 Flesch, T. K., Wilson, J. D., Harper, L. A., Crenna, B. P., and Sharpe, R. R.: Deducing ground-to-
377 air emissions from observed trace gas concentrations: A field trial, *J. Appl. Meteorol.*, 43, 487-
378 502, 10.1175/1520-0450(2004)043<0487:DGEFOT>2.0.CO;2, 2004.
- 379 Glaz, P., Bartosiewicz, M., Laurion, I., Reichwaldt, E. S., Maranger, R., and Ghadouani, A.:
380 Greenhouse gas emissions from waste stabilisation ponds in Western Australia and Quebec
381 (Canada), *Water Research*, 101, 64-74, <https://doi.org/10.1016/j.watres.2016.05.060>, 2016.
- 382 Guisasola, A., de Haas, D., Keller, J., and Yuan, Z.: Methane formation in sewer systems, *Water
383 Res.*, 42, 1421-1430, 10.1016/j.watres.2007.10.014, 2008.
- 384 He, X., Li, H., Chen, J., Wang, H., and Lu, L.: Quantifying greenhouse gas emissions from
385 wastewater treatment plants: A critical review, *Environ. Sci. Ecotechnol.*, 27, 100606,
386 <https://doi.org/10.1016/j.ese.2025.100606>, 2025.
- 387 Hernandez-Paniagua, I. Y., Ramirez-Vargas, R., Ramos-Gomez, M. S., Dendooven, L., Avelar-
388 Gonzalez, F. J., and Thalasso, F.: Greenhouse gas emissions from stabilization ponds in
389 subtropical climate, *Environ. Technol.*, 35, 727-734, 10.1080/09593330.2013.848910, 2014.
- 390 IPCC. *Climate Change 2021: The Physical Science Basis*, 2021.
- 391 Jensen, M. B., Møller, J., Mønster, J., and Scheutz, C.: Quantification of greenhouse gas
392 emissions from a biological waste treatment facility, *Waste Manag.*, 67, 375-384,
393 <https://doi.org/10.1016/j.wasman.2017.05.033>, 2017.
- 394 Laubach, J. and Kelliher, F. M.: Methane emissions from dairy cows: Comparing open-path
395 laser measurements to profile-based techniques, *Agri. Forest Meteorol.*, 135, 340-345, 2005.



- 396 Li, M., Duan, L., Li, S., Wang, D., Gao, Q., Yu, H., Zhang, J., and Jia, Y.: Differences in greenhouse
397 gas emissions and microbial communities between underground and conventionally
398 constructed wastewater treatment plants, *Bioresour. Technol.*, 396, 130421,
399 <https://doi.org/10.1016/j.biortech.2024.130421>, 2024.
- 400 Liu, J., Liu, S., Chen, X., Sun, S., Xin, Y., Liu, L., and Xia, X.: Strong CH₄ emissions modulated by
401 hydrology and bed sediment properties in Qinghai-Tibetan Plateau rivers, *J. Hydrol.*, 617,
402 129053, <https://doi.org/10.1016/j.jhydrol.2022.129053>, 2023.
- 403 Mohsenpour, S. F., Hennige, S., Willoughby, N., Adeloje, A., and Gutierrez, T.: Integrating
404 micro-algae into wastewater treatment: A review, *Sci. Total Environ.*, 752, 142168,
405 10.1016/j.scitotenv.2020.142168, 2021.
- 406 Moore, D. P., Li, N. P., Wendt, L. P., Castañeda, S. R., Falinski, M. M., Zhu, J.-J., Song, C., Ren, Z.
407 J., and Zondlo, M. A.: Underestimation of Sector-Wide Methane Emissions from United States
408 Wastewater Treatment, *Environ. Sci. Technol.*, 57, 4082-4090, 10.1021/acs.est.2c05373, 2023.
- 409 Morales-Rico, P., Ramos-Diaz, J., Mendoza-León, E., Silva-Olmedo, F., and Thalasso, F.: A
410 simplified open flux chamber method for the measurement of greenhouse gas emissions from
411 activated sludge reactors, *J. Water Clim. Chang.*, 15, 2127-2140, 10.2166/wcc.2024.580, 2024.
- 412 NGER: National Greenhouse and Energy Reporting (Measurement) Determination 2008, 2022.
- 413 Nguyen, N. T., Vo, T. S., Tran-Nguyen, P. L., Nguyen, M. N., Pham, V. H., Matsushashi, R., Kim, K.,
414 and Vo, T. T. B. C.: A comprehensive review of aeration and wastewater treatment, *Aquaculture*,
415 591, 741113, <https://doi.org/10.1016/j.aquaculture.2024.741113>, 2024.
- 416 Parravicini, V., Filali, A., Delre, A., Gutierrez, O., and Duan, H.: Full-scale quantification of N₂O
417 and CH₄ emissions from urban water systems, *Quantification and Modelling of Fugitive
418 Greenhouse Gas Emissions from Urban Water Systems*, 91, 2022.
- 419 Reinelt, T., Delre, A., Westerkamp, T., Holmgren, M. A., Liebetrau, J., and Scheutz, C.:
420 Comparative use of different emission measurement approaches to determine methane
421 emissions from a biogas plant, *Waste Manag.*, 68, 173-185,
422 <https://doi.org/10.1016/j.wasman.2017.05.053>, 2017.
- 423 Samuelsson, J., Delre, A., Tumlin, S., Hadi, S., Offerle, B., and Scheutz, C.: Optical technologies
424 applied alongside on-site and remote approaches for climate gas emission quantification at a
425 wastewater treatment plant, *Water Res.*, 131, 299-309,
426 <https://doi.org/10.1016/j.watres.2017.12.018>, 2018.
- 427 Sims, A., Gajaraj, S., and Hu, Z.: Nutrient removal and greenhouse gas emissions in duckweed
428 treatment ponds, *Water Res.*, 47, 1390-1398, <https://doi.org/10.1016/j.watres.2012.12.009>,
429 2013.
- 430 Song, C., Zhu, J.-J., Willis, J. L., Moore, D. P., Zondlo, M. A., and Ren, Z. J.: Methane Emissions
431 from Municipal Wastewater Collection and Treatment Systems, *Environ. Sci. Technol.*, 57,
432 2248-2261, 10.1021/acs.est.2c04388, 2023.
- 433 Søvik, A. K. and Kløve, B.: Emission of N₂O and CH₄ from a constructed wetland in
434 southeastern Norway, *Sci. Total Environ.*, 380, 28-37,
435 <https://doi.org/10.1016/j.scitotenv.2006.10.007>, 2007.
- 436 Thorpe, A. K., O'Handley, C., Emmitt, G. D., DeCola, P. L., Hopkins, F. M., Yadav, V., Guha, A.,
437 Newman, S., Herner, J. D., Falk, M., and Duren, R. M.: Improved methane emission estimates
438 using AVIRIS-NG and an Airborne Doppler Wind Lidar, *Remote Sens. Environ.*, 266, 112681,
439 <https://doi.org/10.1016/j.rse.2021.112681>, 2021.
- 440 Uggetti, E., Garcia, J., Lind, S. E., Martikainen, P. J., and Ferrer, I.: Quantification of greenhouse
441 gas emissions from sludge treatment wetlands, *Water Res.*, 46, 1755-1762,
442 <https://doi.org/10.1016/j.watres.2011.12.049>, 2012.
- 443 Ye, L., Porro, J., and Nopens, I.: Quantification and Modelling of Fugitive Greenhouse Gas
444 Emissions From Urban Water Systems, IWA Publishing, 10.2166/9781789060461, 2022.
- 445 Yver Kwok, C. E., Müller, D., Caldow, C., Lebègue, B., Mønster, J. G., Rella, C. W., Scheutz, C.,
446 Schmidt, M., Ramonet, M., Warneke, T., Broquet, G., and Ciais, P.: Methane emission estimates



447 using chamber and tracer release experiments for a municipal waste water treatment plant,
448 Atmos. Meas. Tech., 8, 2853–2867, 10.5194/amtd-8-2957-2015, 2015.

449

450

451

452

453

454

455

456

457

458

459

460

461

462

463

464

465

466

467

468

469

470

471

472

473

474

475

476

477

478



479 **Figures**

480 **Figure 1**



481

482 **Figure 1.** The layout of experimental site with one upwind open-path laser (light blue line with triangles), and
483 two downwind open-path lasers (green and purple for summer campaign, green and blue for winter campaign).
484 The Red triangle shows the weather station location during the summer campaign, while the dark blue triangle
485 shows the weather station location during the winter campaign. (Source: Image ©2024 Airbus, Google Earth).

486

487

488

489

490

491

492

493

494

495

496

497

498

499

500

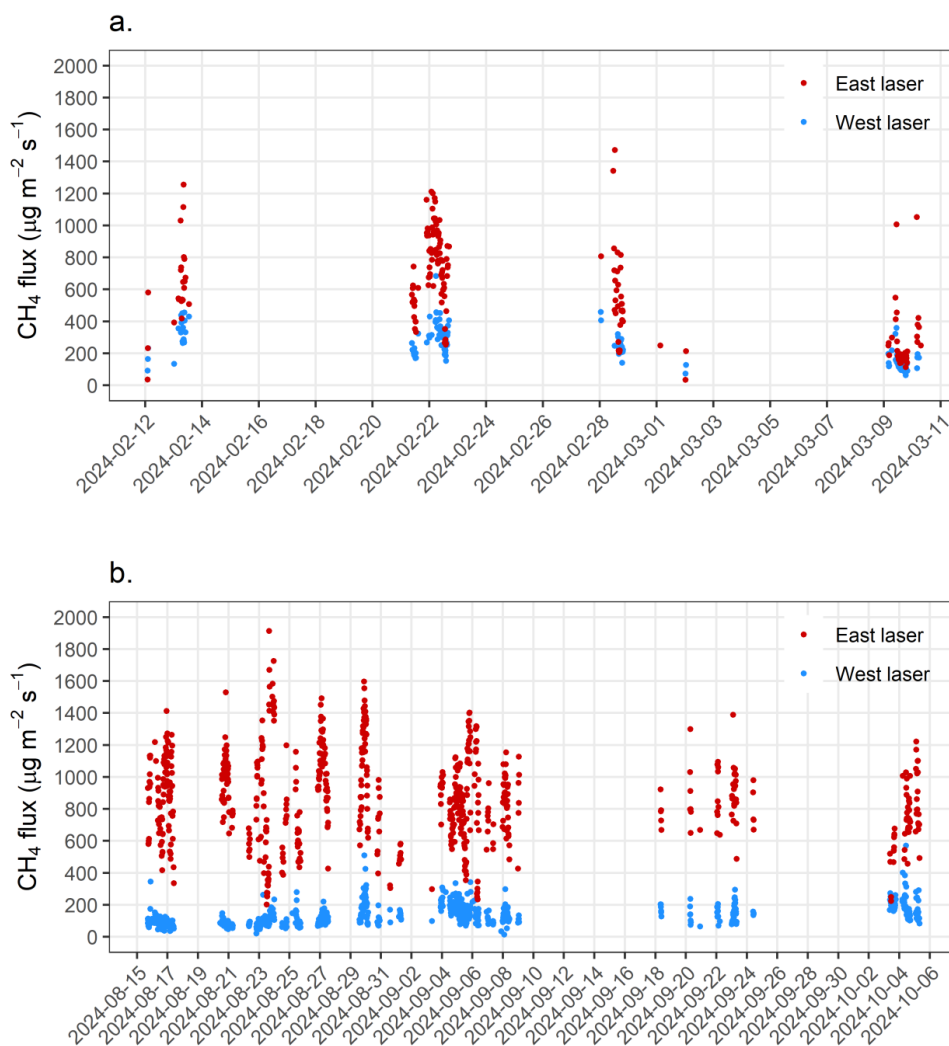
501

502



503 **Figure 2**

504



505

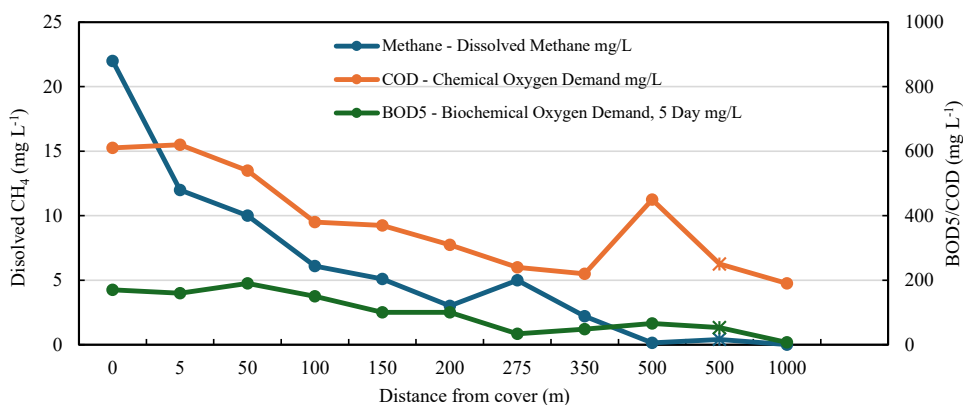
506 **Figure 2.** Fifteen-minute CH₄ fluxes from western (blue) and eastern area (red) of sewage treatment 25W Pond 1
507 measured over the summer season (a) from 12 February to 10 March 2024, and the winter season (b) from 15
508 August to 5 October 2024 in Victoria, Australia.

509

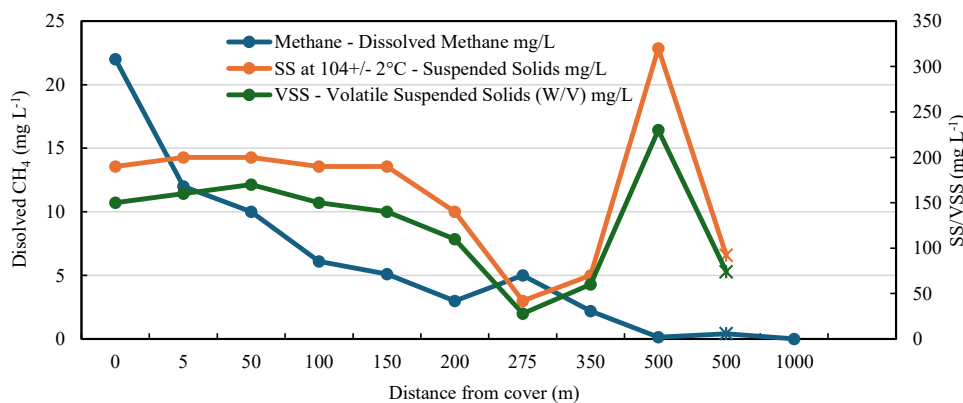
510



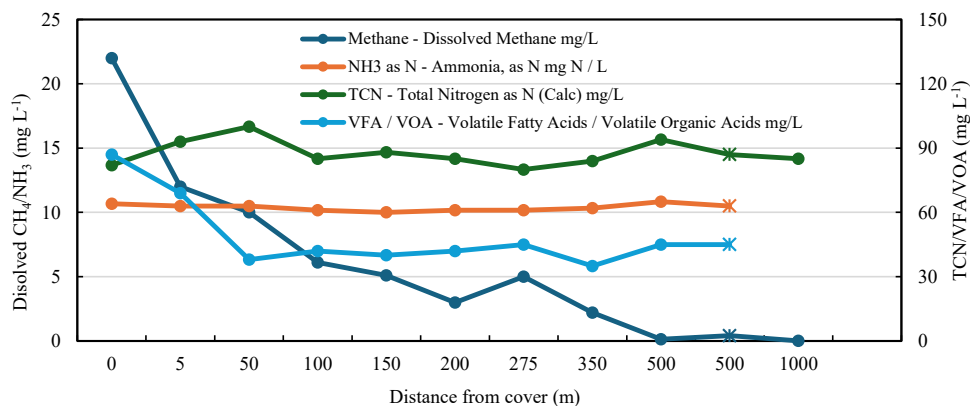
511 Figure 3



512



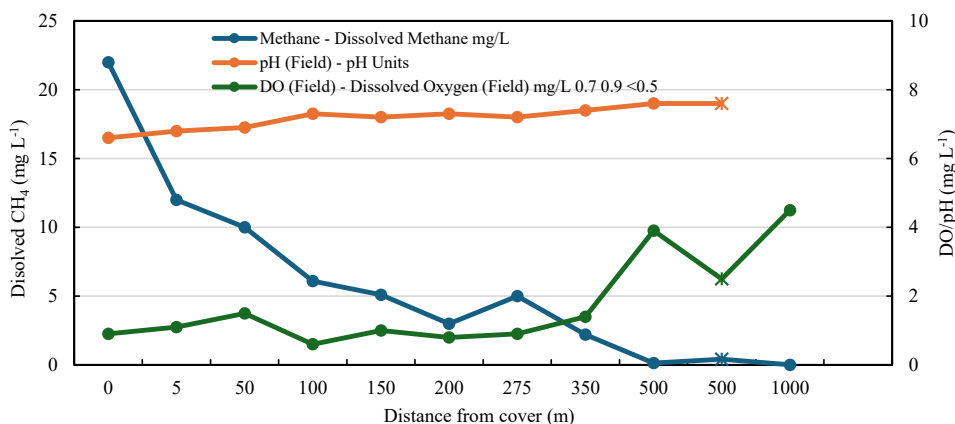
513



514

515

516



517

518 **Figure 3.** Variations of dissolved methane, BOD, COD, SS, VSS, NH₃, TCN, VFA, pH, and dissolved oxygen
519 shown with increasing distance from the cover area. Wastewater samples were collected by drone along the middle
520 part of Pond 1 between 10:00–12:30 on the 10 September 2024 at 5, 50, 100, 150, 200, 275, 350, and 500 m from
521 the cover, and extra samples were also collected at the PotCod, the jetty area (marked with an “ж”) and Pond 1
522 outlet (0, 500, and 1000 m from the cover, respectively) on the same day.

523

524

525

526

527

528

529

530

531

532

533

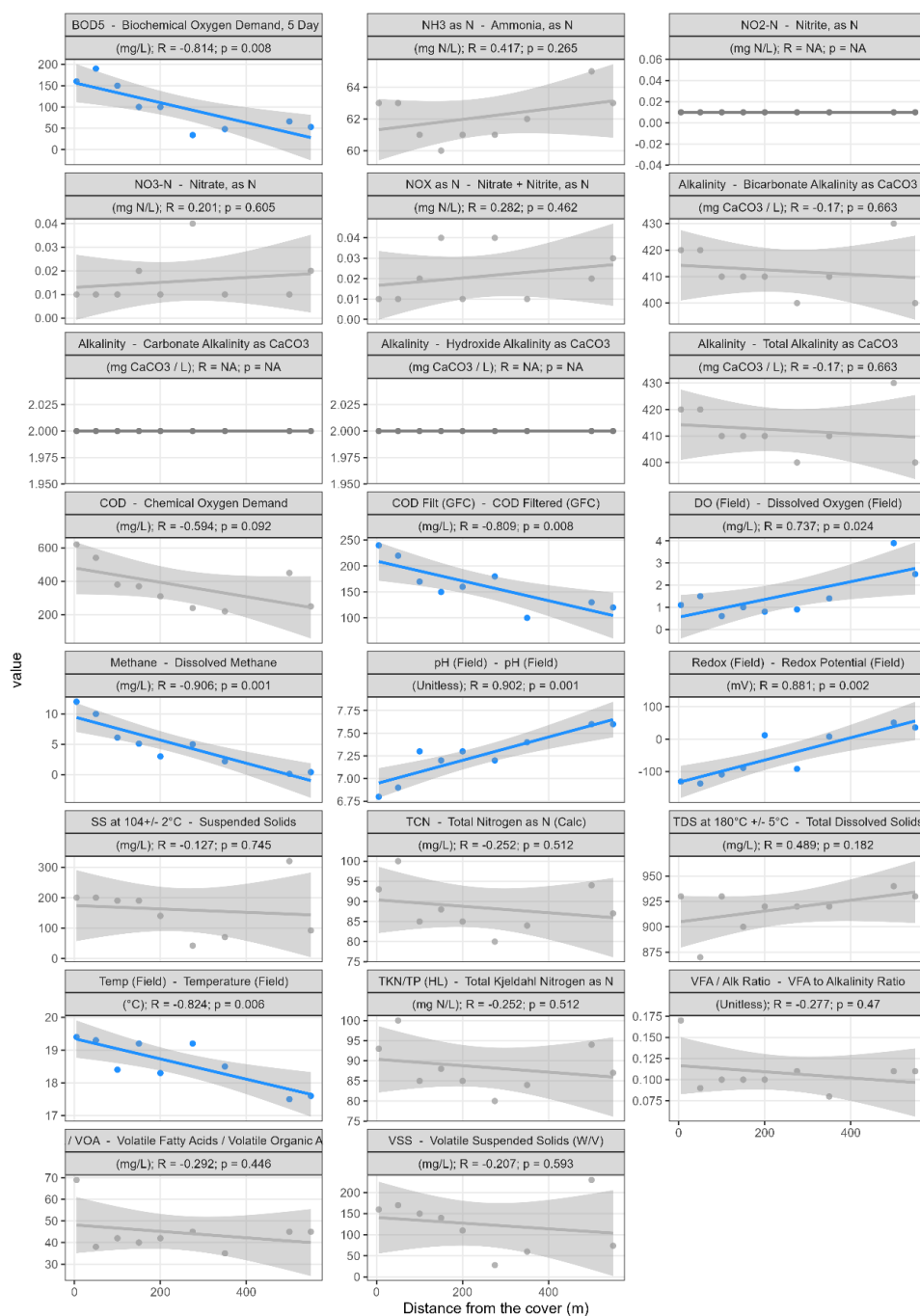
534

535

536



537 Figure 4



538

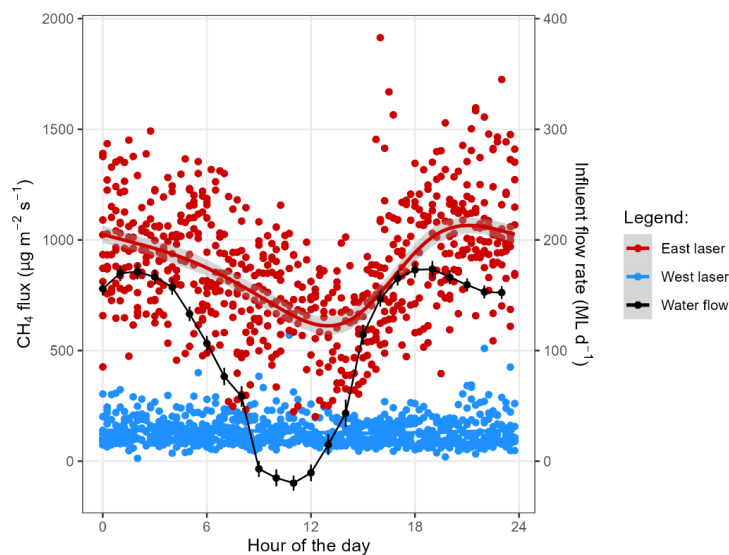
539 **Figure 4.** Correlations between wastewater sample contents including dissolved methane, BOD, COD, SS, VSS,
 540 N-NH₃, TCN, VFA, pH, and dissolved oxygen and the distance from the anaerobic cover. Samples were collected



541 by drone along the middle part of Pond 1 between 10:00–12:30 on the 10 September 2024 at 5, 50, 100, 150, 200,
542 275, 350, 500 m from the anaerobic cover, extra samples were also collected at the PotCod and the jetty area (0
543 and 500 m from the cover) on the same day. Linear correlation coefficient (R) and P value are also shown.

544

545 Figure 5



546

547 **Figure 5.** 24-h diurnal variation of average wastewater flow rate and CH_4 fluxes during a winter campaign at 25W
548 Pond 1 from 15 August to 5 October 2024.

549

550

551

552

553

554

555

556

557

558

559

560



561 **Tables**

562 Table 1

563 **Table 1. Daily average of CH₄ flux (μg m⁻² s⁻¹) from the western pond area and eastern pond area measured**
 564 **at 25W Pond 1 from 8 February to 10 March 2024 (summer campaign) and 15 August to 5 October 2024**
 565 **(winter campaign). The accumulative GHG flux (CO₂ equivalent, CO₂-e) and accumulative methane per**
 566 **net load COD (ΔCOD) (kgCH₄ t⁻¹ΔCOD) are also shown.**

	Summer campaign		Winter campaign	
	Western pond area emissions (μg m ⁻² s ⁻¹)	Eastern pond area emissions (μg m ⁻² s ⁻¹)	Western pond area emissions (μg m ⁻² s ⁻¹) [§]	Eastern pond area emissions (μg m ⁻² s ⁻¹)
	252.01 (n = 139)	582.06 (n = 185)	134.68 (n = 797)	874.19 (n = 692)
Daily averaged flux (μg m ⁻² s ⁻¹)	50 %:50 % weight	417.04	Low range High range	319.6 378.7
	417.0		349.1	
Daily averaged Pond 1 flux (t day ⁻¹) ^δ	8.79		7.36	
Daily ΔCOD load (t day ⁻¹) [#]	36.58		41.25	
kgCH ₄ t ⁻¹ ΔCOD	240.3		178.4	
<hr/>				
Average Pond 1 CH ₄ emission (μg m ⁻² s ⁻¹) [#]	381.1			
Annual Pond 1 CH ₄ emission (t) [#]	2,947.9			
Annual GHG emissions (tCO ₂ -e yr ⁻¹) [‡]	79,593.3			

567 ^δ, the 25W Pond 1 area is 244,007 m²

568 [§] n, the number of good measurements [§] the s.e. for the mean represents the total uncertainty [#] COD, chemical
 569 oxygen demand. The mean daily net load of COD (ΔCOD) is 379.8, 306.2 mg L⁻¹ for winter and summer
 570 campaign, respectively. ΔCOD is determined by the difference between the average influent COD value measured
 571 at the east end and the average wastewater COD value at the outlet, ΔCOD_{summer} = 445.0 – 138.8 = 306.2 mg L⁻¹,
 572 ΔCOD_{winter} = 581.3 – 201.4 = 379.8 mg L⁻¹. Daily flow rate is 108.6, 119.5 ML day⁻¹ for winter and summer
 573 campaign, respectively. The daily net load of COD in t day⁻¹ = 379.8 × 10⁻⁹ mg L⁻¹ × 108.6 × 10⁶ L day⁻¹ = 41.25
 574 tCOD day⁻¹ (winter campaign). For summer campaign, the daily net load of COD in t day⁻¹ = 306.2 × 10⁻⁹ mg L⁻¹ ×
 575 119.5 × 10⁶ L day⁻¹ = 36.58 tCOD day⁻¹.

576 [#] total uncertainty associated with the averages is 20.7 and 20.4 % for the eastern and western measurements,
 577 respectively. The total uncertainty for both campaigns is 20.5 % using the equation: square root of
 578 (0.5*(20.7 %)²+0.5*(20.4 %)²) and is dominated by the inverse dispersion model uncertainty.

579 [‡] annual Pond 1 emission (t) × 27 of global warming potential for CH₄

580

581

582



583 Table 2

584 **Table 2. Flux measurements from this study compared to NGRS reporting, the mass balance of liquid**
 585 **emission and methane production from the anaerobic Pot.**

	Summer campaign tCO ₂ -e yr ⁻¹	Winter campaign tCO ₂ -e yr ⁻¹
NGERS Reporting based on emissions factor for FY2024 [‡]		25,079
NGERS Reporting based on emissions factor for FY2023 [‡]		48,607
Mass balance (not including sludge) emissions	25,019	23,298
OP laser spectroscopy flux measurements (upper)	89854	81599
Average annual flux measurements (upper)		85,727
OP laser spectroscopy flux measurements (lower)	89,854	68,852
Average annual flux measurements (lower)		79,353
		12,128 CH ₄ t yr ⁻¹
		339,573 tCO₂-e yr⁻¹
		25.3%
		23.4%

586 [‡]NGERS, national greenhouse and energy reporting scheme

587